Article

Post-resection delivery of a TLR7/8 agonist from a biodegradable scaffold achieves immune-mediated glioblastoma clearance and protection against tumor challenge in mice

Elizabeth G. Graham-Gurysh [1], Ryan N. Woodring[1], Sean R. Simpson[1], Sophie E. Mendell[1], Nicole Rose Lukesh[1], Erik S. Pena[2], Kathryn M. Moore[2], Luis A. Ontiveros-Padilla[1], Aaron T. Hendricksen[1], Alexandra M. Lopez[1], Grace L. Williamson [1], Connor T. Murphy [1], Christopher J. Genito [3], Kaitlyn A. Hipp[4,5], Garima Singh [1], William C. Zamboni[4,5], Shawn D. Hingtgen [1], Peter E. Fecci[6,7,8], Eric M. Bachelder[1] & Kristy M. Ainslie [1,2,3] ✉

Glioblastoma is an aggressive brain cancer with a dismal prognosis despite current therapeutic interventions. Surgical tumor resection, standard-of-care for glioblastoma, not only results in the reduction of tumor burden, but also has profound immunostimulatory effects, offering a unique opportunity to break local immune tolerance and mount an effective anti-tumor immune response. Here, we explore the effect of local controlled release of resiquimod, a TLR7/8 agonist, from a biodegradable polymer scaffold implanted at the time of tumor resection. We find that treatment leads to the clearance of residual post-resection tumor, improved survival, and subsequent protection from tumor challenges in orthotopic mouse models of glioma. In addition, the controlled release of resiquimod from the scaffold boosts the resection-mediated disruption to the tumor microenvironment, leading to an early inflammatory innate immune response both in the brain and cervical lymph node, followed by an influx of lymphocytes. Thus, we show that sustained local TLR7/8 agonism at the time of tumor resection represents a promising approach for the treatment of glioblastoma.

Glioblastoma (GBM) is a highly invasive and aggressive brain tumor. Even with standard-of-care therapy including surgical resection, radiation, and chemotherapy, local tumor recurrence and mortality is almost 100%[1–3]. In an effort to combat local tumor recurrence, extensive research has evaluated drug delivery systems implanted directly in the post-surgical cavity to deliver chemotherapies locally[4–6]. A clinical

example of this is Gliadel®, an FDA-approved biodegradable polymeric wafer that delivers carmustine directly into the brain tissue of the tumor resection cavity[7,8]. However, limitations with drug diffusion kinetics and a high rate of adverse events have restricted its efficacy[9].

Immunotherapies are a promising alternative to cytotoxic chemotherapies, and their success against other malignancies has sparked

1

exploration for GBM. Unfortunately, GBM immunotherapy faces a steep uphill battle[10–16]. GBM has one of the most immunosuppressive tumor microenvironments (TME)[17,18], but also elicits a variety of systemic immune derangements, such as T cell sequestration in the bone marrow[19]. Additionally, GBM has a low tumor mutational burden, which complicates the identification of neoantigens[20]. Moreover, single antigen approaches are often confounded by the heterogeneous nature of GBM[21–23].

One strategy for combatting the immunosuppressive TME has been to target microglia and macrophages, which are major mediators of anti-inflammatory signaling in GBM[24,25]. Microglia and macrophages express substantial levels of Toll-like receptors (TLR), innate immune sensors, which recognize pathogen-associated molecular patterns[24]. Activation of TLRs has been a useful therapeutic avenue for cancer therapy, capable of shifting immunosuppressive cells towards a pro-inflammatory phenotype as well as activating both innate and subsequently adaptive immune responses against tumors[26]. However, preclinical investigations into TLR agonists for GBM therapy have had varied success[27,28].

Surgical debulking of the tumor is a core component of GBM clinical treatment and results in significant immunological effects. Studies have shown that trauma caused by surgery and the resulting immediate inflammation can later exacerbate immunosuppression within the TME[29,30]. However, in the immediate term, GBM surgery reduces myeloid-derived suppressor cells (MDSC) and promotes recruitment of effector T cells to the brain[31,32]. This suggests that perioperative immunotherapy could both capitalize on the reduced tumor burden and disrupted TME, as well as potentially mitigate concerns of later surgical-induced tumorigenesis[33]. Indeed, neoadjuvant administration of checkpoint blockade has already demonstrated some promise in GBM[34].

Immunotherapy delivered directly to the tumor site has proven safer and more effective than systemic administration[35]. By focusing delivery near the tumor, local immune tolerance can be disrupted, facilitating systemic antitumor immunity. One way this can be achieved is by loading an immunotherapeutic within a biodegradable polymer implant[36–39]. Through diffusion and polymer matrix degradation, the immunotherapeutic is released at a sustained rate, creating a local inflammatory response and chemotactic gradient to recruit leukocytes to the brain. Additionally, the polymer matrix can shield the encapsulated immunotherapeutic and limit drug degradation in situ[40,41].

In this study, we formulate a small molecule TLR7/8 agonist, resiquimod, within a biodegradable polymer scaffold for controlled release of the agonist over several days. This scaffold is implanted in the brain at the time of tumor resection to harness the immunostimulatory effects of surgical tumor resection and generate an antitumor immune response. We find that delivery of resiquimod via scaffold increases and prolongs resiquimod retention in the brain compared to bolus injection of resiquimod. In two orthotopic murine models, GL261 and CT2A, scaffold therapy improves survival and leads to the formation of immune memory and protection from tumor challenge. Additionally, we observe that scaffold-mediated delivery of resiquimod leads to an immunostimulatory environment in the brain and draining lymph nodes and stimulates systemic T cell trafficking. These results suggest that sustained, local immune stimulation coupled with tumor resection offers an innovative strategy for GBM immunotherapy.

Results

Sustained resiquimod elicits tumor clearance, memory

To probe the benefit of sustained local TLR7/8 stimulation within the context of tumor resection, resiquimod was formulated within an acetalated dextran (Ace-DEX) polymer scaffold for controlled release. Ace-DEX is a biodegradable polymer with adjustable degradation rates created by modifying hydroxyl groups of dextran with cyclic and acyclic acetals[42–44]. Resiquimod was incorporated within an Ace-DEX polymer scaffold through electrospinning. The resulting resiquimod-loaded scaffold, Ace-Resi, was composed of randomly aligned microfibers and displayed zero-order release of resiquimod over 7 days in vitro (Fig. 1 A, B). The scaffold was completely degraded by 14 days in vitro (Supplementary Fig. 1A).

The pharmacokinetics of Ace-Resi (100 μg) scaffolds compared to a bolus injection of 100 μg resiquimod in phosphate buffered saline (Sol. Resi) were evaluated in healthy mice (no intracranial tumor). Ace-Resi scaffolds were implanted or Sol. Resi was injected within a sham resection cavity in the right hemisphere of the brain. This is important, as studies have shown that resection can greatly affect drug diffusion[45,46]. Ace-Resi scaffolds resulted in a higher concentration of resiquimod in the whole brain compared to bolus injection throughout a seven-day period (Fig. 1C), increasing the area under the curve (AUC) in the brain by 19-fold (Supplementary Table 1). Plasma resiquimod concentration for both the scaffold and bolus injection was maximum at the 1 hour timepoint, tapering off quickly (Supplementary Fig. 1B). When comparing resiquimod concentrations in whole brain to plasma out to day 7, the concentration in the brain was 8.0 to 18.9-fold higher than in the plasma for Ace-Resi, which is evidence for prolonged local drug retention mediated by the scaffold (Supplementary Fig. 1C). In contrast, bolus injection only exhibited a 4.6-fold higher concentration of resiquimod in the brain at 1 hour, and by 6 hours it was roughly equivalent to plasma. Additionally, we evaluated the retention of resiquimod in Ace-Resi scaffolds removed from brains during this in vivo study to compare with in vitro conditions (Supplementary Fig. 1D). We found that resiquimod is released slightly faster in vivo, but with a similar kinetic profile to in vitro.

In a mouse model of GBM resection, a pilot study was done with GL261-mCh-Luc tumors to evaluate the feasibility and dose of perioperative treatment with bolused soluble resiquimod and Ace-Resi (Supplementary Fig. 2A). Two weeks after implantation, tumors were debulked, and mice were treated with control scaffolds (Ace-Blank), resiquimod-loaded scaffolds (Ace-Resi) at a dose of 10 or 100 μg of resiquimod, or a bolus injection of 100 μg resiquimod (Sol. Resi). 80% and 60% of mice treated with Ace-Resi, at low and high doses respectively, achieved durable tumor suppression as measured by bioluminescence and survival (Fig. 1D, Supplementary Fig. 2B–F). However, all mice treated with the control scaffold and bolus resiquimod succumbed to tumor burden. Ultimately, bolus injection of resiquimod offered no survival advantage, while sustained exposure to resiquimod did. Treatment with Ace-Resi was well tolerated, with mice experiencing ~5–10% transient weight loss for two days following treatment (Supplementary Fig. 2K, L).

To examine immune memory formation, the long-term survivors from both low and high dose Ace-Resi groups were challenged with GL261-mCh-Luc tumors in the contralateral hemisphere 10 weeks after tumor resection and treatment. All mice demonstrated protection from challenge indicating an immune memory response (Fig. 1E, Supplementary Fig. 2G–J). One week after a second tumor challenge, T cell infiltration in the brain was assessed, and an increase in T cell counts and frequency was observed in long-term survivors previously treated with Ace-Resi (Fig. 1F, Supplementary Fig. 2M). Additionally, when Ace-Resi long-term survivors were combined, there was an increase in CD8^{+} to CD4^{+} ratio compared to naïve mice bearing tumors (Supplementary Fig. 2N), indicating an increased cytotoxic T cell response.

These results suggested that controlled release via scaffold was more important than the dose of resiquimod in achieving a durable anti-tumor response. A second study was conducted with an intermediate dose, Ace-Resi (50 μg) (Supplementary Fig. 3A). Similarly to the prior study, this treatment was well tolerated, and 50% of mice treated with Ace-Resi during tumor resection achieved durable tumor
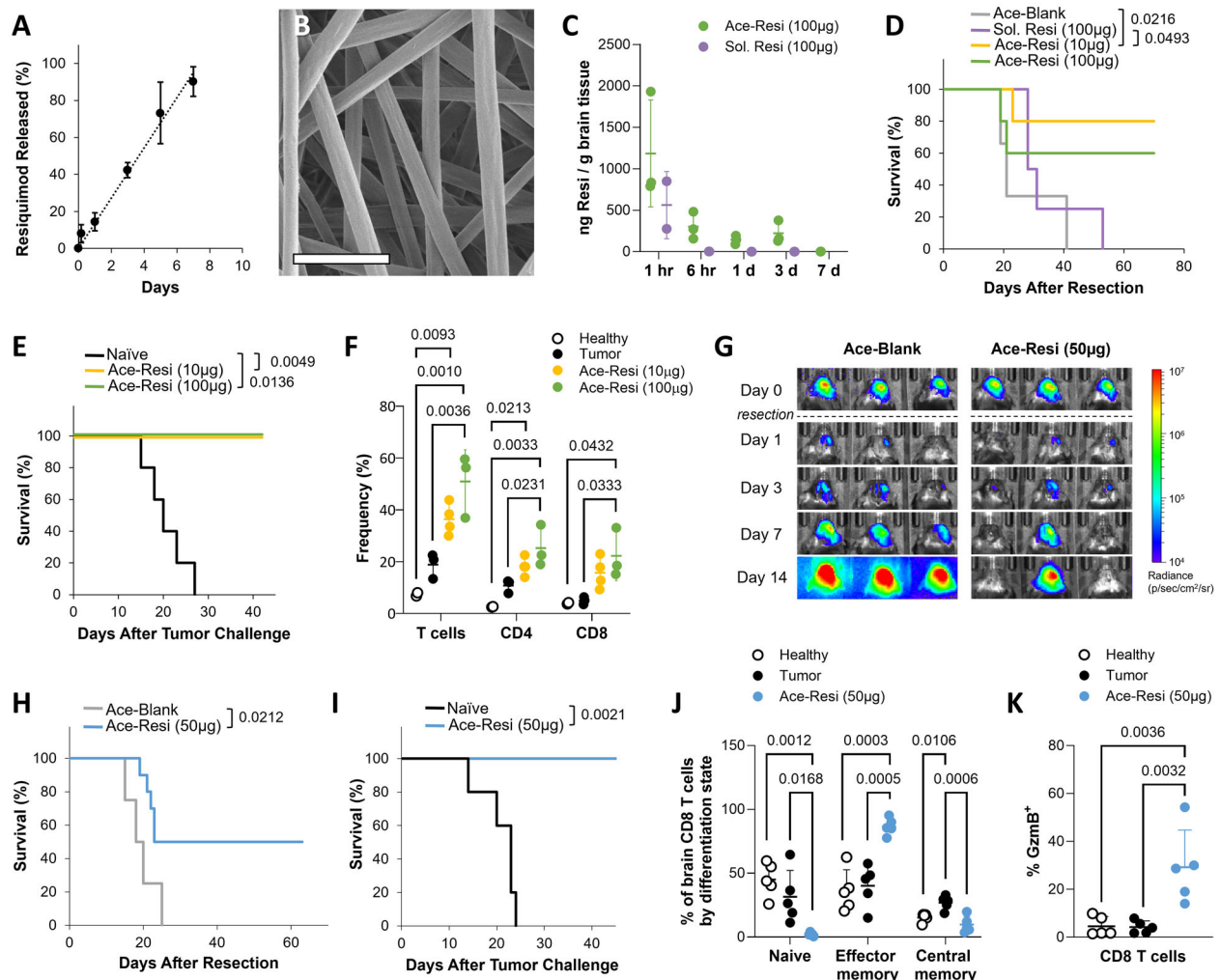
Fig. 1 | GL261 study and pharmacokinetics. A Release of resiquimod from polymer scaffold in vitro. $n = 3$ scaffold samples per timepoint, one independent experiment. Data are presented as mean ± SD. **B** Scanning electron micrograph of Ace-Resi scaffold. Scale bar is 5 μm. **C** Concentration of resiquimod in the brain over time for mice treated with 100 μg of resiquimod via Ace-Resi or bolus injection (Sol. Resi). $n = 3$ mice per timepoint, one independent experiment. Data are presented as mean ± SD. **D** Survival of mice after tumor resection and treatment with Ace-Blank ($n = 3$ mice), soluble resiquimod 100 μg ($n = 4$ mice), Ace-Resi 10 μg ($n = 5$ mice), or Ace-Resi 100 μg ($n = 5$ mice). One independent experiment. P-values, log-rank test. **E** Survival of long-term survivors after the first tumor challenge. Ace-Resi 10 μg ($n = 4$ mice), Ace-Resi 100 μg ($n = 3$ mice), with naïve mice ($n = 5$ mice) utilized as a control. P-values, log-rank test. **F** Frequency of T cells in the brain 1 week after the second tumor challenge. healthy (no tumor, $n = 2$ mice) and tumor ($n = 3$ mice) controls, and Ace-Resi 10 μg ($n = 4$ mice), Ace-Resi 100 μg ($n = 3$ mice). One

independent experiment. Data are presented as mean ± SD. P-value, one-way ANOVA, Tukey's multiple comparisons test. **G** Representative bioluminescent images of mice after tumor resection. **H** Survival of mice after tumor resection and treatment with vehicle Ace-Blank ($n = 4$ mice) or Ace-Resi 50 μg ($n = 10$ mice). One independent experiment. P-values, log-rank test. **I** Survival of long-term survivors after the first tumor challenge. Ace-Resi 50 μg ($n = 5$ mice) with naïve mice ($n = 5$) utilized as a control. One independent experiment. P-values, log-rank test. **J** Differentiation state of CD8+ T cells in the brain one week after the second tumor challenge. $n = 5$ mice for each group, one independent experiment. Data are presented as mean ± SD. P-value, one-way ANOVA, Tukey's multiple comparisons test. **K** Percentage of CD8+ T cells in the brain that are granzyme B+ (GzmB) one week after second tumor challenge. $n = 5$ mice per group, one independent experiment. Data are presented as mean ± SD. P-value, one-way ANOVA, Tukey's multiple comparison test.

suppression (Fig. 1 G, H, Supplementary Fig. 3B, C, F, and G). These mice were also protected from tumor challenge (Fig. 1I, Supplementary Fig. 3D, E, and H). One week after a second tumor challenge, T cell infiltration in the brain was assessed, and a significant increase in CD4+ and CD8+ T cell frequency was observed in long-term survivors (Supplementary Fig. 3I). In evaluating the phenotype of the T cells, long-term survivors from the Ace-Resi (50 μg) group displayed decreased frequency of naïve and central memory phenotype coupled with increased frequency of effector memory phenotype (Fig. 1J, Supplementary Fig. 3J). Mice treated with the Ace-Resi scaffolds also had an increase in the percentage of granzyme B (GzmB+) CD8+ T cells (Fig. 1K). This corroborates the indication of an increased cytotoxic T cell response in long-term survivors.

For a more comprehensive evaluation, we repeated a therapeutic study in mice bearing CT2A-Luc tumors, a model shown to be more immunologically cold than GL261 (Fig. 2A)[32]. Like the GL261 model, all mice treated with the control scaffold or bolus resiquimod succumbed to tumor burden. In contrast, perioperative treatment with Ace-Resi not only extended median survival (21.5 days compared to 12.5 days for Ace-Blank control) but also resulted in complete tumor eradication in 31.6% of mice as measured by bioluminescence and survival (Fig. 2B, C, Supplementary Fig. 4A–E). Long-term survivors challenged with CT2A-Luc tumors in the contralateral hemisphere demonstrated complete protection from tumor challenge (Fig. 2D, E, Supplementary Fig. 4F–H). Brain lymphocytes were evaluated by flow cytometry one week after a second tumor challenge. Mice treated with the Ace-Resi
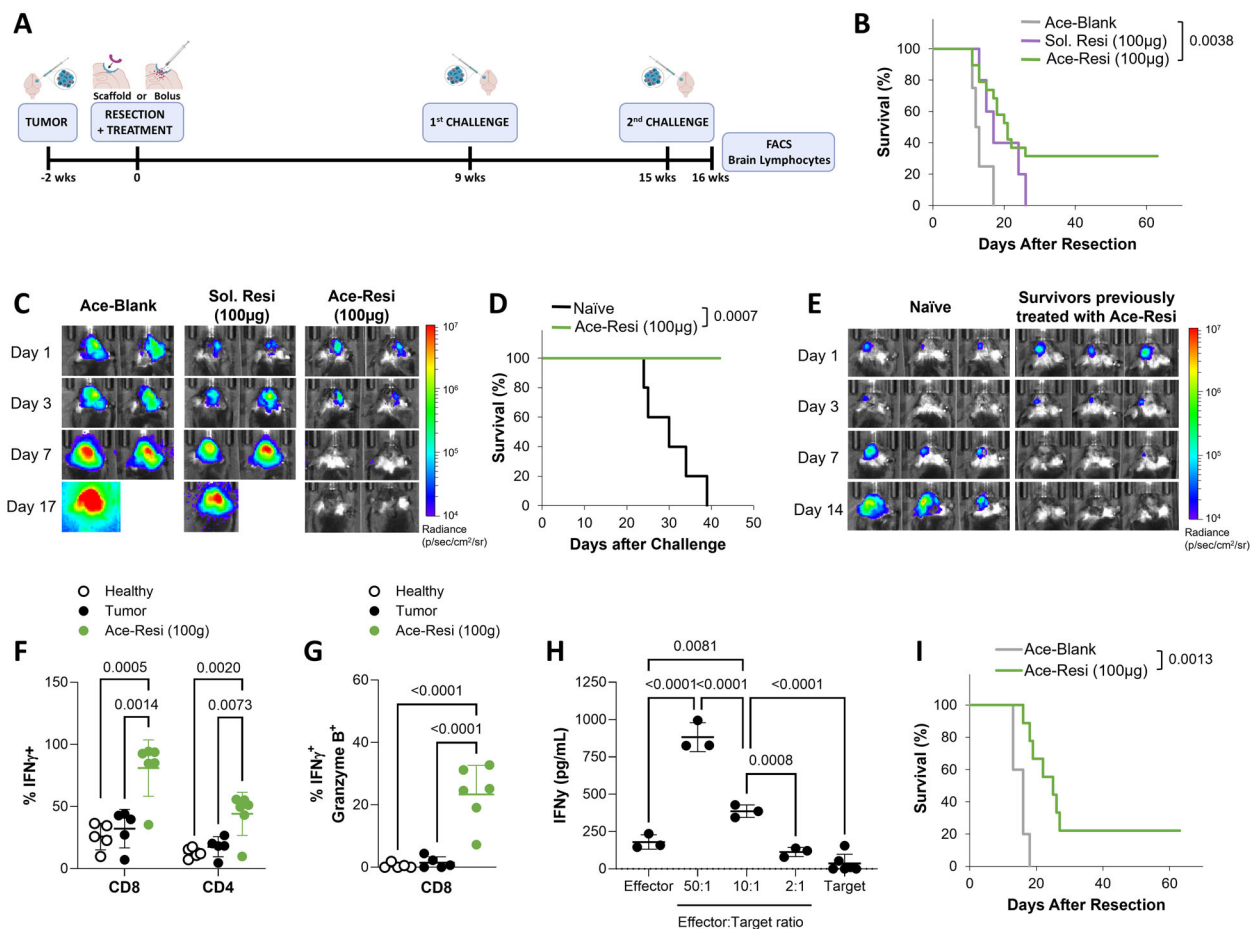
Fig. 2 | CT2A and EO771 study. A Timeline of study design. CT2A-Luc tumor implanted and resected 2 weeks later (day 0). Ace-Resi or bolus resiquimod treatment applied immediately following tumor resection. Surviving mice were challenged at 9 weeks and then again at 15 weeks. Mice euthanized at 16 weeks for brain lymphocyte analysis. **B** Survival of mice after tumor resection and treatment with Ace-Blank ($n = 4$ mice), soluble resiquimod 100 μg ($n = 5$ mice), or Ace-Resi 100 μg ($n = 19$ mice). One independent experiment. *P*-value, log-rank test. **C** Representative bioluminescent images of mice after tumor resection. **D** Survival of mice after the first tumor challenge. Ace-Resi 100 μg ($n = 6$ mice) with naïve mice ($n = 5$) as controls. One independent experiment. *P*-value, log-rank test. **E** Representative bioluminescent images of mice following the first tumor challenge. **F** Percent of T cells that are positive for IFNγ. Healthy (no tumor, $n = 5$ mice) and tumor ($n = 5$ mice)

controls, and $n = 6$ Ace-Resi 100 μg mice, one independent experiment. Data are presented as mean ± SD. *P*-value, one-way ANOVA, Tukey's multiple comparisons test. **G** CD8⁺ T cells that are positive for both IFNγ and granzyme B. Healthy (no tumor, $n = 5$ mice) and tumor ($n = 5$ mice) controls, and $n = 6$ Ace-Resi 100 μg mice, one independent experiment. Data are presented as mean ± SD. *P*-value, one-way ANOVA, Tukey's multiple comparisons test. **H** IFNγ in the supernatant of effector cells (isolated from $n = 3$ long-term survivors and pooled together) co-cultured with CT2A-Par cells ('target cells') for 24 hours in $n = 3$ or $n = 6$ individual wells. One independent experiment. Data are presented as mean ± SD. *P*-value, one-way ANOVA, Tukey's multiple comparisons test. **I** Survival of mice after EO771 tumor resection and treatment with Ace-Blank ($n = 5$ mice) or Ace-Resi 100 μg ($n = 9$ mice), one independent experiment. *P*-value, log-rank test.

group demonstrated increased frequencies and counts of CD8⁺ T cells (Supplementary Fig. 4I, J), interferon gamma (IFNγ⁺) CD8⁺ and CD4⁺ T cells (Fig. 2F, Supplementary Fig. 4K), and polyfunctional IFNγ⁺ GzmB⁺ CD8⁺ T cells (Fig. 2G, Supplementary Fig. 4L) compared to tumor-bearing mice and healthy (no tumor) controls. These results indicated that the implantation of Ace-Resi into the tumor resection cavity induced a robust cytotoxic CD8⁺ T cell response that correlated strongly with protection against tumor rechallenge.

Ace-Resi efficacy was repeated in a CT2A-Par mouse model, a tumor line without any reporter proteins, and displayed comparable survival benefit (Supplementary Fig. 5A, B). Importantly, effector cells isolated from these long-term survivors and co-cultured with CT2A-Par cells released IFNγ in a dose-dependent manner (Fig. 2H), whereas effector cells isolated from naïve (non-tumor-bearing) mice did not (Supplementary Fig. 5C). This indicates that Ace-Resi induces cytolytic activity in an antigen-specific manner in the absence of reporter protein luciferin.

The efficacy of Ace-Resi was also evaluated with a model of breast cancer brain metastasis (Supplementary Fig. 5D). Established EO771

tumors in the brain were resected and treated with Ace-Resi (100 μg) or Ace-Blank. Treatment with Ace-Resi increased median survival (25 days compared to 16 days for Ace-Blank control) and resulted in 22.2% long term survivors (Fig. 2I). This suggests that Ace-Resi treatment could be more broadly applicable and might be similarly effective against brain metastasis of other solid tumors where resection is the standard-of-care.

Ace-Resi reshapes immunity, promotes T cell trafficking

We next sought to understand the early immunological events after Ace-Resi treatment compared to healthy (no tumor), tumor (no resection), and resection and Ace-Blank controls. On set days after surgical resection of CT2A-Luc tumors and perioperative scaffold treatment, mice were euthanized, and immune populations were analyzed using flow cytometry (Fig. 3A). As seen in Fig. 3B and Supplementary Fig. 6, 1 day after Ace-Resi treatment, the number of leukocytes in the brain exhibited a precipitous drop, relative to the unresected tumor-bearing control. While resection with Ace-Blank
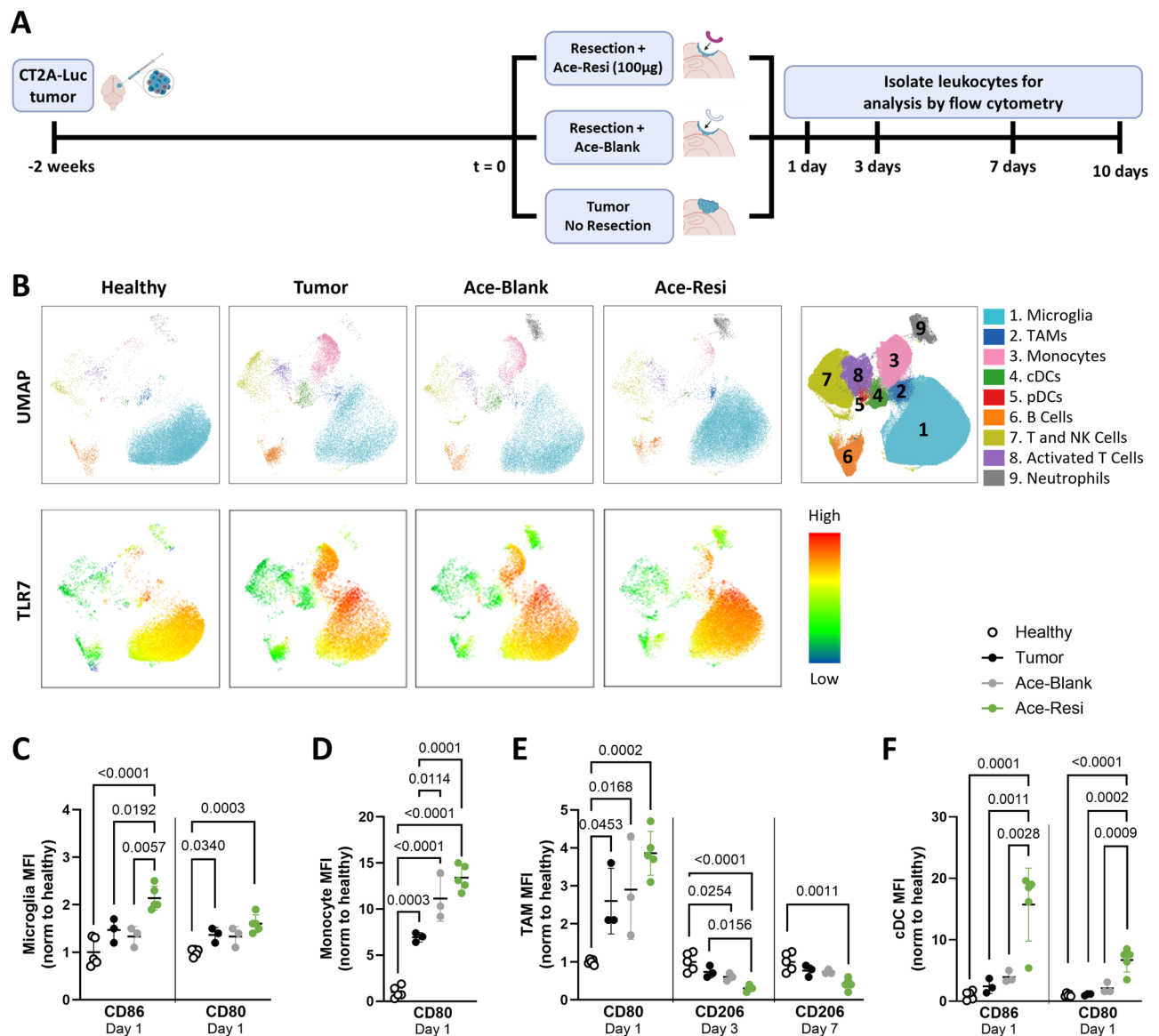
Fig. 3 | Ace-Resi remodels the brain immune environment. A Timeline of study design. CT2A-Luc tumors were implanted 2 weeks prior; mice were randomized to treatment group. Mice were euthanized days 1, 3, 7, and 10 after treatment and organs harvested for flow analysis. Healthy mice were included as a control. B UMAP of 9 leukocyte populations in the brain on Day 1, with corresponding heatmap of TLR7 expression. $n = 5$ healthy, $n = 3$ tumor, $n = 3$ Ace-Blank, and $n = 5$ Ace-Resi mice, one independent experiment. C Mean fluorescence intensity (MFI) of CD86 and CD80 in microglia on Day 1. $n = 5$ healthy, $n = 3$ tumor, $n = 3$ Ace-Blank, and $n = 5$ Ace-Resi mice, one independent experiment. Data are presented as mean ± SD. P-value, one-way ANOVA, Tukey's multiple comparisons test. D MFI of

CD80 in monocytes on Day 1. $n = 5$ healthy, $n = 3$ tumor, $n = 3$ Ace-Blank, and $n = 5$ Ace-Resi mice, one independent experiment. Data are presented as mean ± SD. P-value, one-way ANOVA, Tukey's multiple comparisons test. E MFI of CD80 on Day 1 and CD206 on Days 3 and 7 in tumor associated macrophages (TAM). $n = 5$ healthy, $n = 3$ tumor, $n = 3$ Ace-Blank, and $n = 5$ Ace-Resi mice, one independent experiment. Data are presented as mean ± SD. P-value, one-way ANOVA, Tukey's multiple comparisons test. F MFI of CD86 and CD80 in conventional dendritic cells (cDC) on Day 1. $n = 5$ healthy, $n = 3$ tumor, $n = 3$ Ace-Blank, and $n = 5$ Ace-Resi mice, one independent experiment. Data are presented as mean ± SD. P-value, one-way ANOVA, Tukey's multiple comparisons test.

scaffold also reduced the number of leukocytes, the effect was less pronounced.

Hierarchical consensus clustering of flow cytometry data by FlowSOM[47] identified nine populations of immune cells in the brain as shown by UMAP (Fig. 3B, Supplementary Figs. 7, 8). Evaluating the frequencies of these populations, one day after resection there is a significant decrease in the frequency of monocytes, conventional dendritic cells (cDC), and plasmacytoid dendritic cells (pDC) for Ace-Resi compared to unresected tumor controls with a corresponding increase in microglia (Supplementary Fig. 8A–D). Ace-Blank displays similar movement in these immune populations, just to a lesser extent than Ace-Resi. We also find that resection leads to a transitory increase

in the neutrophil population with or without Ace-Resi (Supplementary Fig. 8E). The frequency of tumor-associated macrophage (TAM) population is significantly higher for the tumor group compared to healthy controls, and it continues to increase with time (Supplementary Fig. 8F). By comparison, tumor resection leads to static TAM levels, and seven days after resection, both Ace-Blank and Ace-Resi groups have significantly lower levels of TAMs. The frequency of activated T cells increases with time for all groups, and ten days after resection, Ace-Blank and Ace-Resi have a significantly higher proportion compared to the tumor group (Supplementary Fig. 8G). The reduction in TAM and increase in activated T cell populations both speak to the benefits of tumor resection.
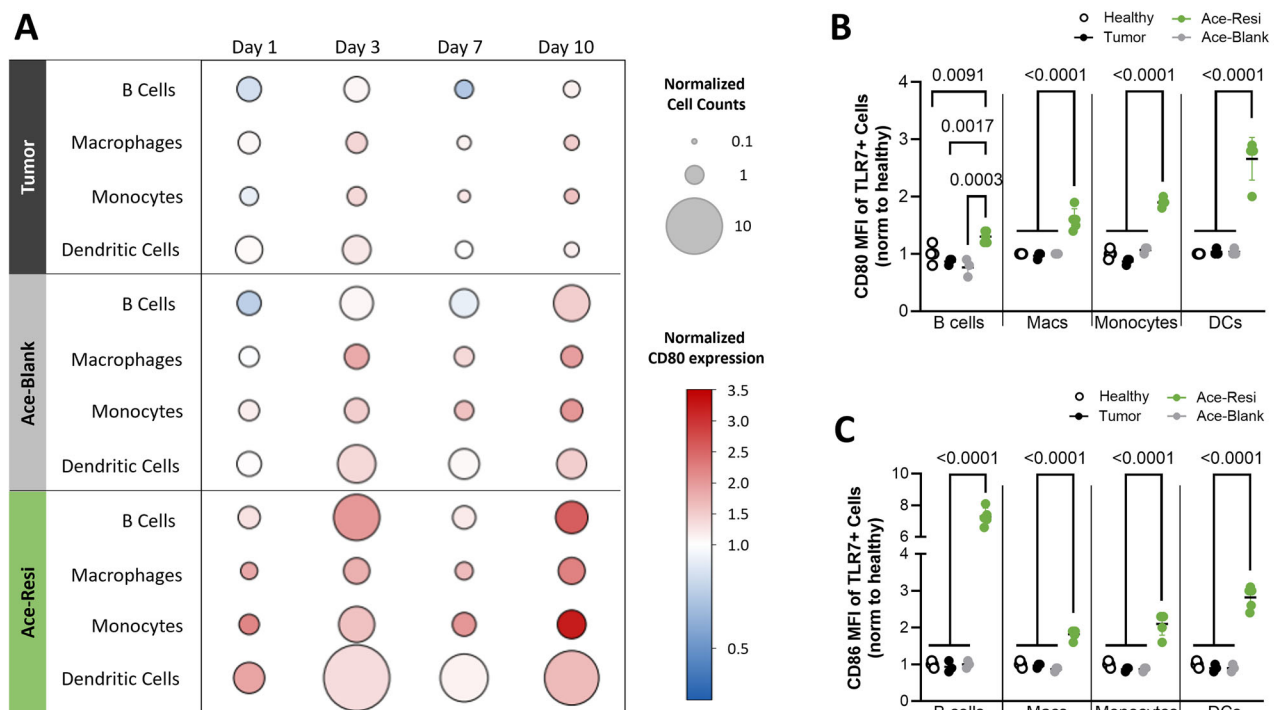
Fig. 4 | Ace-Resi leads to cell trafficking and immunostimulatory environment in cervical lymph node. A Bubble plot of antigen-presenting cells (APC) in the cervical lymph node over time with normalized cell counts represented by dot size and normalized CD80 mean fluorescence intensity (MFI) represented by shading. Cell counts and CD80 MFI are normalized to healthy controls. **B** MFI of CD80 and for TLR7 + APC populations on Day 1. $n = 5$ healthy, $n = 3$ tumor, $n = 3$ Ace-Blank, and $n = 5$ Ace-Resi mice, one independent experiment. Data are presented as mean ± SD. P-value, one-way ANOVA, Tukey's multiple comparisons test. **C** MFI of CD86 for TLR7 + APC populations on Day 1. $n = 5$ healthy, $n = 3$ tumor, $n = 3$ Ace-Blank, and $n = 5$ Ace-Resi mice, one independent experiment. Data are presented as mean ± SD. P-value, one-way ANOVA, Tukey's multiple comparisons test.

Overlaying TLR7 expression onto these populations we observe that microglia, monocytes, and TAMs are the most abundant populations with high expression of TLR7 (Fig. 3B). Mice treated with Ace-Resi display microglia activation as seen by an increase in CD86 mean fluorescence intensity (MFI) compared to all other groups and an increase in CD80 compared to healthy (Fig. 3C). The presence of a tumor alone appears to stimulate monocytes as the tumor group has an increased CD80 MFI compared to healthy controls; however, tumor resection leads to further stimulation of this population as evidenced by increased CD80 MFI for Ace-Blank and Ace-Resi mice compared to the tumor group (Fig. 3D). Similar to monocytes, all groups have an increase in TAM CD80 MFI on day 1 compared to healthy; however, the Ace-Resi group also exhibits a decrease MFI of the immunosuppressive marker CD206 on days 3 and 7 (Fig. 3E). We also observed strong activation of CD80 and CD86 in cDCs and B cell populations for mice treated with Ace-Resi, suggesting that Ace-Resi scaffold also stimulates populations with moderate TLR7 expression (Fig. 3F, Supplementary Fig. 8J). In summary, these changes illustrate that resection and Ace-Resi create conditions that promote recruitment and infiltration of peripheral immune cells[48].

Evaluating the cervical lymph nodes (cLN), we find Ace-Resi induces cell trafficking and stimulation of antigen-presenting cells (APC, Fig. 4A, Supplementary Fig. 9). Ace-Resi induced trafficking is most significant for DCs, which exhibit a sustained response with increased frequency and counts days 3 through 10 (Supplementary Fig. 9D, I). B cells, macrophages, and monocytes also demonstrate an increase in counts 3 days after resection (Supplementary Fig. 9F–H). Notably, mice treated with Ace-Resi show strong activation with increased CD80 and CD86 MFI for B cells, macrophages, monocytes, and DCs (Fig. 4A, Supplementary Fig. 9P–W). Assessing these populations for TLR7 expression, we find that the percentage TLR7+ APCs

increases for all groups compared to healthy controls (Supplementary Fig. 10). Though only the Ace-Resi group displays an increase in costimulatory CD86 and CD80 expression for these TLR7+ populations (Fig. 4B, C).

Examining the early lymphocyte responses to Ace-Resi implantation in the brain, the frequency of highly activated natural killer (NK) cells positive for IFNγ and GzmB was significantly enhanced on both days 1 and 7 in mice (Fig. 5A, B). By day 7, these mice also exhibited high counts of double positive IFNγ⁺ GzmB⁺ NK cells (Supplementary Fig. 11A), despite the large drop in brain leukocyte counts immediately following scaffold implantation. Interestingly, the TME of unresected tumor-bearing mice also exhibited large numbers of activated NK cells, potentially indicating an active anti-tumor immune response. However, these mice also have high frequencies and counts of regulatory T cell (Treg) populations (Fig. 5C, D, Supplementary Fig. 11B). Consistent with a beneficial role for resection, both Ace-Blank and Ace-Resi treated mice exhibited a significant reduction of Tregs in the brain in contrast to unresected tumor mice (Fig. 5C, D, Supplementary Fig. 11B). However, Ace-Blank mice saw the frequency and counts of Tregs increase and ultimately match unresected tumor mice within 10 days after resection, while Ace-Resi mice maintained the lower frequency and counts out to day 10. Tregs can potently suppress conventional effector T cell responses, and their induction and recruitment to the TME is a major mechanism by which tumors escape immune destruction[49].

Finally, we examined the phenotype and function of CD8⁺ T cells in the brain. Surprisingly, no significant differences were observed in the frequency of IFNγ⁺ or IFNγ⁺ GzmB⁺ CD8⁺ T cells in the brains of any of the groups that received tumors (Supplementary Fig. 11C–E), and CD8⁺ T cell counts were highest in untreated tumor-bearing mice (Supplementary Fig. 11C). In fact, there is a positive correlation
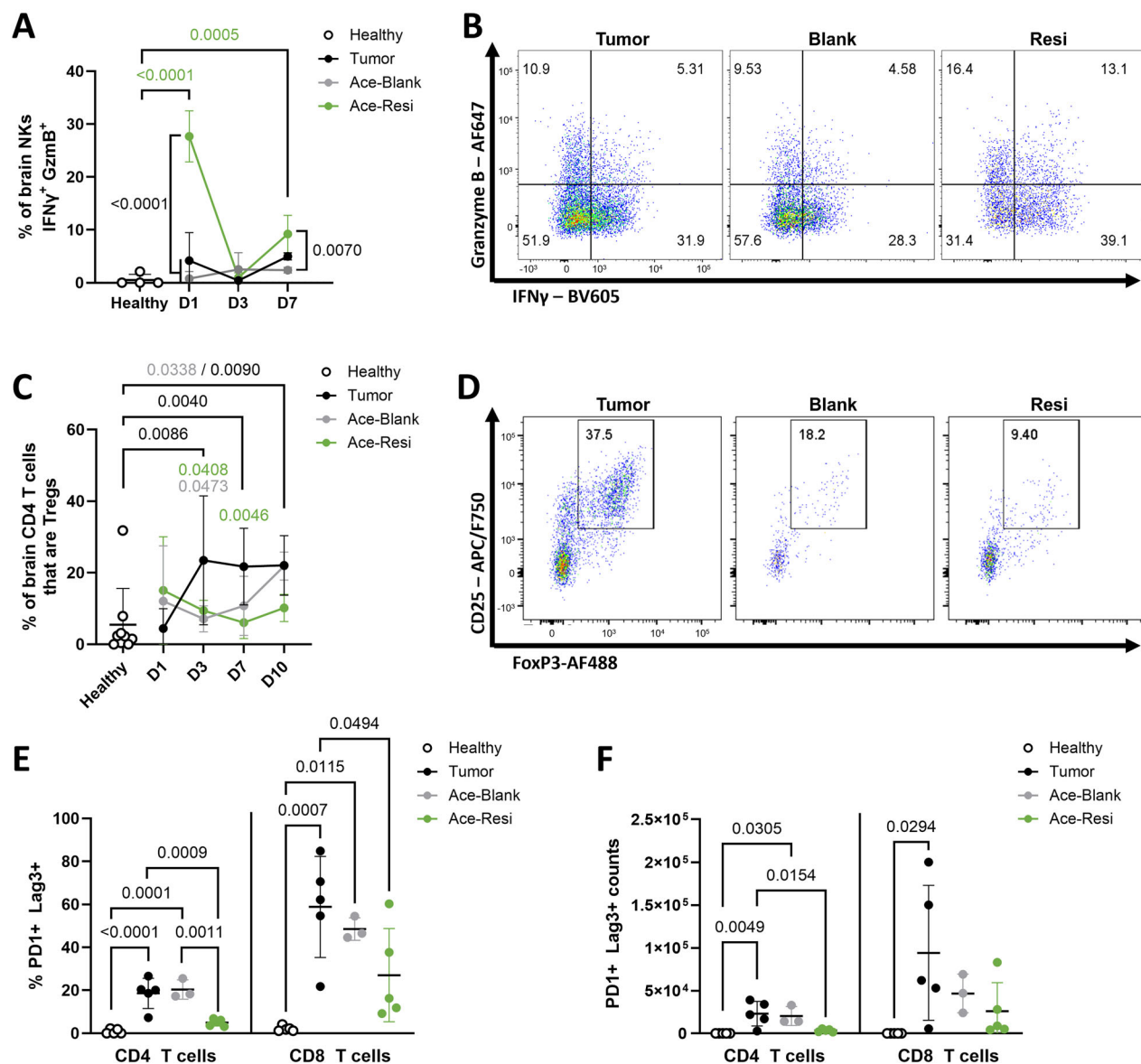
Fig. 5 | Ace-Resi promotes NK activation, decreases T-regs, and reduces T cell exhaustion in the brain. A Percent of natural killer (NK) cells in the brain that are positive for both IFNγ and granzyme B (GzmB) over time. $n = 4$ healthy, $n = 3$ tumor, $n = 3$ Ace-Blank, and $n = 5$ Ace-Resi mice, one independent experiment. Data are presented as mean ± SD. *P*-value, one-way ANOVA at each timepoint, Tukey's multiple comparisons test with respect to healthy and tumor controls. **B** Representative day 7 dot plots demonstrating IFNγ and GzmB expression of NK cells in the brain. **C** Percent of CD4^{+} T cells that are positive for T-reg markers (Foxp3^{+} CD25^{+}) in the brain over time. $n = 9$ healthy, $n = 5–7$ tumor, $n = 3–6$ Ace-Blank, and $n = 5–11$ Ace-Resi mice at each timepoint, two independent experiments.

Data are presented as mean ± SD. *P*-value, one-way ANOVA at each timepoint, Tukey's multiple comparisons test with respect to healthy and tumor controls. **D** Representative day 7 dot plots of Tregs in the brain. **E** Frequency of exhausted (PD1^{+} Lag3^{+}) CD8^{+} and CD4^{+} T cells on Day 10. $n = 5$ healthy, $n = 5$ tumor, $n = 3$ Ace-Blank, and $n = 5$ Ace-Resi mice, one independent experiment. Data are presented as mean ± SD. *P*-value, one-way ANOVA, Tukey's multiple comparisons test. **F** Counts of exhausted (PD1^{+} Lag3^{+}) CD8^{+} and CD4^{+} T cells on Day 10. $n = 5$ healthy, $n = 5$ tumor, $n = 3$ Ace-Blank, and $n = 5$ Ace-Resi mice, one independent experiment. Data are presented as mean ± SD. *P*-value, one-way ANOVA, Tukey's multiple comparisons test.

between tumor burden, as measured by bioluminescence, and CD8^{+} T cell counts in the brain for tumor and Ace-Blank groups (Supplementary Fig. 11F, G). However, Ace-Resi group follows a different pattern, where CD8^{+} T cell counts increase with time but with no correlation to tumor burden (Supplementary Fig. 11H). One mechanism that can restrict T cell activity is exhaustion; chronic high-level T cell receptor signaling in the TME can cause T cells to become hyporesponsive to further stimulation, limiting their ability to mediate tumor clearance. This exhausted state is correlated with upregulation of multiple cell surface inhibitory receptors, including PD-1 and LAG-3[50]. The frequency and counts of exhausted T cells (PD1^{+} Lag3^{+}), both CD4^{+} and CD8^{+}, steadily increase with time for Ace-Blank and unresected tumor

groups (Supplementary Fig. 12A–D). By contrast, Ace-Resi treatment restrains exhaustion, seen most clearly at Day 10 (Fig. 5E, F).

In addition to local brain and cLN immune-modulation, we observed rapid systemic effects of Ace-Resi treatment. One day following resection and Ace-Resi implantation, we noted robust CD69 upregulation on T cells, NK cells, and B cells in the spleen, bone marrow, and cLN (Fig. 6A, B, Supplementary Fig. 13A–H). In addition to being a marker of T cell activation[51], CD69 is rapidly upregulated by T cells in response to IFN-I, like IFNβ[52]. Notably, mice treated with Ace-Resi exhibit a marked spike in serum IFN-β and TNF at 2 hours, which returned to baseline by 24 hours (Supplementary Fig. 14A, B). This was followed by an increase in IFNγ, which peaked on day 3 before
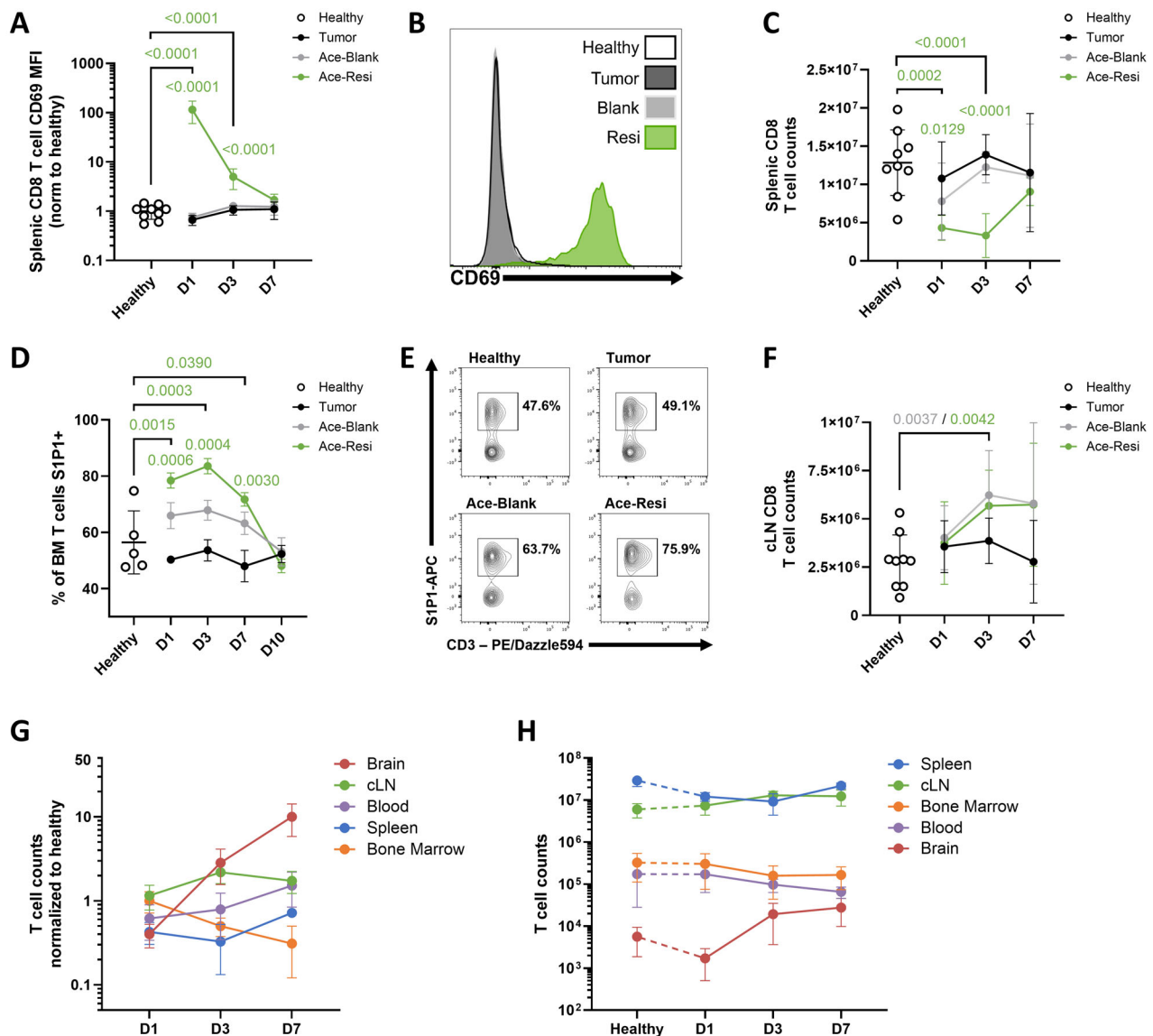
Fig. 6 | Ace-Resi induces systemic signaling and T cell re-localization. A Healthy control normalized mean fluorescence intensity (MFI) of CD69 staining on splenic CD8^{+} T cells. $n = 9$ healthy, $n = 6$-7 tumor, $n = 6$ Ace-Blank, and $n = 10$-11 Ace-Resi mice for each timepoint, two independent experiments. Data are presented as mean ± SD. *P*-value, one-way ANOVA at each timepoint, Tukey's multiple comparisons test with respect to healthy and tumor controls. **B** Day 1 representative histograms of CD69 on splenic CD8^{+} T cells. **C** CD8^{+} T cell counts in the spleen. $n = 9$ healthy, $n = 6$-7 tumor, $n = 6$ Ace-Blank, and $n = 10$-11 Ace-Resi mice for each timepoint, two independent experiments. Data are presented as mean ± SD. *P*-value, one-way ANOVA at each timepoint, Tukey's multiple comparisons test with respect to healthy and tumor controls. **D** Percentage of S1P1 + T cells from bone marrow (BM) after resection. $n = 5$ healthy, $n = 3$-4 tumor, $n = 3$ Ace-Blank, and $n = 5$ Ace-Resi mice for each timepoint, one independent experiment. Data are presented as mean ± SD. *P*-value, one-way ANOVA at each timepoint, Tukey's multiple

comparisons test with respect to healthy and tumor controls. **E** Representative day 1 histogram of S1P1 + T cells from bone marrow (BM) after resection. **F** CD8^{+} T cell counts in the cervical lymph node (cLN) over time. $n = 9$ healthy, $n = 6$-7 tumor, $n = 6$ Ace-Blank, and $n = 10$-11 Ace-Resi mice for each timepoint, two independent experiments. Data are presented as mean ± SD. *P*-value, one-way ANOVA at each timepoint, Tukey's multiple comparisons test. **G** T cell counts from mice treated with Ace-Resi in specific organs normalized to $n = 9$ healthy controls. $n = 10$-11 mice for each timepoint, two independent experiments. Data are presented as mean ± 95% CI. **H** T cell counts from healthy controls and mice treated with Ace-Resi in specific organs. $n = 9$ healthy and $n = 10$-11 Ace-Resi mice for each timepoint, two independent experiments. Data are presented as mean ± 95% CI. Counts from spleen, cLN, and brain are total counts. Counts from blood are per μL. Counts from the bone marrow are total counts from one femur.

returning to baseline on day 7 (Supplementary Fig. 14C). We observed transient T cell depletion in the spleens of Ace-Resi treated mice (Fig. 6C), which was not seen in Ace-Blank. Acute viral infection causes similar temporary effects, which are associated with IFN-I-dependent re-localization to the lymph nodes and other tissues[52].

Intracranial tumors have been shown to induce T cell sequestration in the bone marrow by downregulating sphingosine-1-phosphate receptor 1 (S1P1), activation of which is required for egress from lymphatic tissue[19]. We observed that Ace-Resi led to a steady decrease in

bone marrow T cell counts, concurrently with an increase in T cells in the brain and cLN (Fig. 6F–H). Ace-Blank resulted in similar effects, but to a lesser degree (Supplementary Fig. 13I). Furthermore, mice treated with Ace-Resi exhibited a significant increase in S1P1 expression on T cells in the bone marrow for seven days compared to healthy and tumor controls (Fig. 6D, E), suggesting that surgical resection and Ace-Resi may free up T cells in the bone marrow for systemic recirculation.

To explore the mechanism of Ace-Resi, therapeutic efficacy against CT2A tumors was evaluated in mice lacking T cells (Nu/Nu)
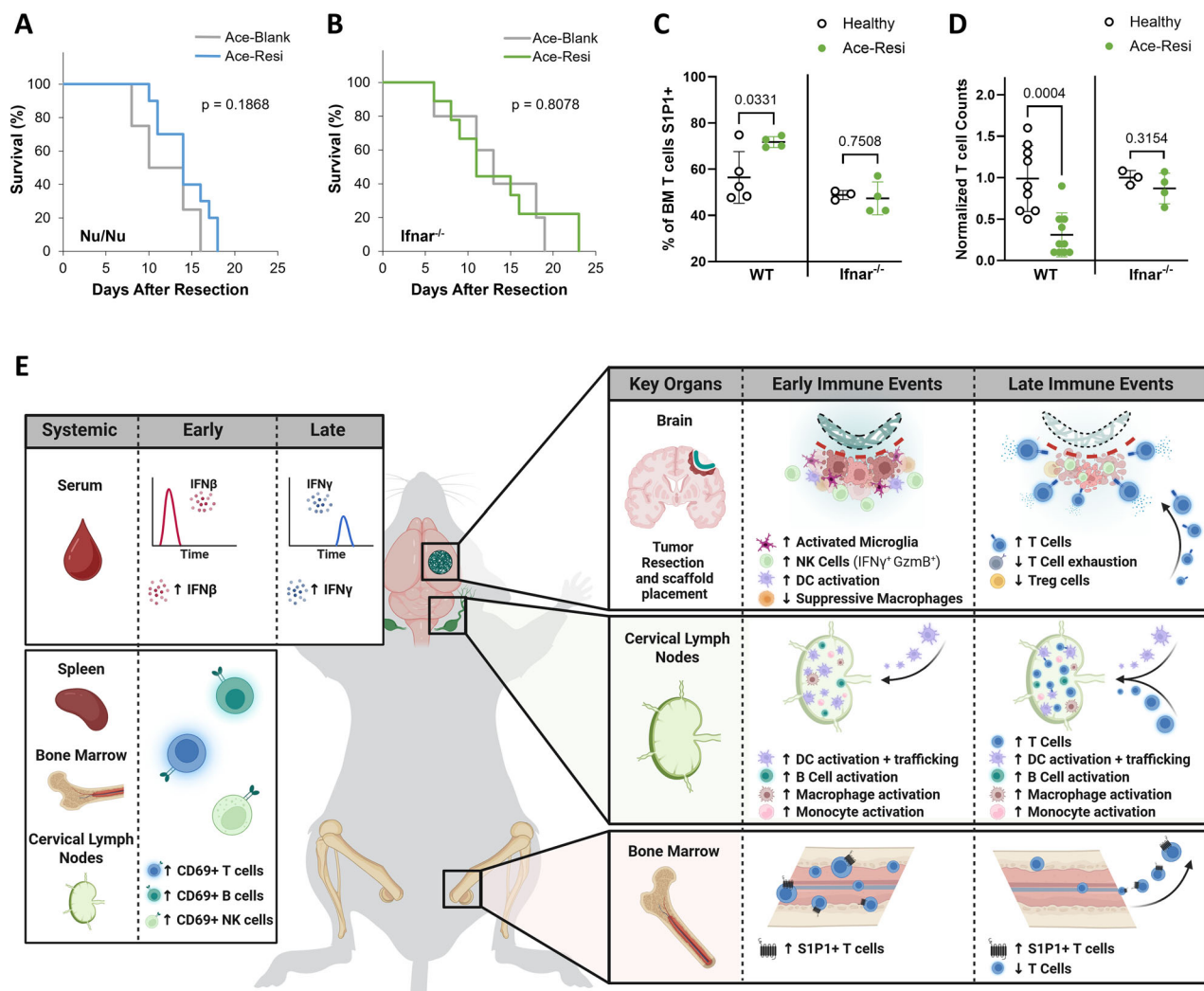
Fig. 7 | Ace-Resi efficacy requires T cells and IFN-I. A Survival of Nu/Nu mice bearing CT2A tumors after resection and treatment with Ace-Blank ($n = 4$ mice), and Ace-Resi ($n = 10$ mice), one independent experiment. *P*-value, log-rank test. **B** Survival of Ifnar$^{-/-}$ mice bearing CT2A tumors after resection and treatment with Ace-Blank ($n = 5$ mice), and Ace-Resi ($n = 9$ mice), one independent experiment. *P*-value, log-rank test. **C** Frequency of bone marrow T cells that are S1P1+ from wildtype C57BL6 (WT) and Ifnar$^{-/-}$ mice comparing healthy (no tumor) controls to mice 7 days after tumor resection and treatment with Ace-Resi. WT: $n = 5$ healthy, $n = 4$ Ace-Resi mice. Ifnar$^{-/-}$: $n = 3$ healthy, $n = 4$ Ace-Resi mice. One independent experiment. *P*-value, two-tailed unpaired *t*-test. **D** Normalized T cell counts in the bone marrow from wildtype C57BL6 (WT) and Ifnar$^{-/-}$ mice comparing healthy (no tumor) controls to mice 7 days after tumor resection and treatment with Ace-Resi.

WT: $n = 9$ healthy, $n = 10$ Ace-Resi mice, two independent experiments. Ifnar$^{-/-}$: $n = 3$ healthy, $n = 4$ Ace-Resi mice, one independent experiment. *P*-value, two-tailed unpaired *t*-test. **E** Perioperative administration of Ace-Resi scaffold resets the immunosuppressive tumor microenvironment: depleting suppressive regulatory T cells (T-reg), decreasing tumor-associated macrophages (TAM), and activating microglia, natural killer (NK) cells, and dendritic cells (DC). An increase in S1P1 allows T cells to traffic out of the bone marrow and to the cervical lymph node where they can be primed by activated DCs and other activated antigen-presenting cells. A wave of CD8^{+} T cells traffics to the brain. These events help mount a robust immune response to clear residual tumor and ultimately lead to protection from tumor challenge.

and interferon receptor knockout mice (Ifnar$^{-/-}$) (Fig. 7A, B, Supplementary Fig. 15). Ace-Resi did not improve survival in either model, indicating that both T cells and interferon signaling are required for Ace-Resi therapeutic benefit. To probe this further, the effect of interferon signaling on T cell trafficking from bone marrow was evaluated in wildtype C57BL6 (WT) mice compared to Ifnar$^{-/-}$ mice. In WT mice, tumor resection and treatment with Ace-Resi led to an increase in frequency of S1P1 expression in T cells and a decrease in T cell counts in the bone marrow. By contrast, T cell counts and S1P1 expression remain the same for Ifnar$^{-/-}$ mice (Fig. 7C, D). This suggests that interferon signaling plays a role in Ace-Resi mediated increase in S1P1 expression on T cells in the bone marrow and the lack of signaling reduces T cell trafficking from the bone marrow.

Discussion

Glioblastoma (GBM) is a highly aggressive brain tumor with a nearly 100% recurrence rate despite standard treatments. Surgical resection is the standard-of-care for GBM and has profound immune effects; however, preclinical evaluations of immunotherapy are rarely studied within this paradigm[53,54]. We investigated the effect of continuous local stimulation of TLR7/8 perioperatively by formulating resiquimod within an Ace-DEX polymer scaffold. Scaffolds were fabricated by electrospinning, which produces a thin, flexible, fibrous material ideal for implantation in the brain[36]. Applying the tunability of Ace-DEX polymer platform, we are able to achieve linear release kinetics over 7 days. This is a slower and more controlled release than most formulated resiquimod evaluated in the literature for similar applications which typically only release over 6–12 hours[55–57].

We observed large differences in the pharmacokinetics of Ace-Resi in the brain versus bolus intracranial injection of resiquimod. Ace-Resi had average of 10-fold increases in local resiquimod concentration in the brain compared to plasma out to 3 days. Reduced systemic delivery of resiquimod is important as many clinical trials with TLR7/8 stimulation have concerns with systemic toxicities[58-60]. Further reduced dosing of resiquimod may still be efficacious, especially considering that we observed similar long-term protection across resiquimod doses (10, 50, and 100 μg).

In this study we find that sustained local release of resiquimod administered at the time of tumor resection can lead to durable tumor suppression that protects mice from a tumor challenge indicating the formation of immune memory response. It appears that the dose of resiquimod applied is not the critical element to mount an anti-tumor response, but rather that the local resiquimod stimulation lasts longer than a bolus administration (>1 h as measured by pharmacokinetics). Further, we found Ace-Resi tumor clearance to be dependent on the presence of T cells and interferon signaling.

In both GL261-mCh-Luc and CT2A-Luc models, bolus injection of soluble resiquimod intracranially did not result in tumor regression or any long-term survivors. This is in contrast to Grauer et al.[28] who reported that soluble intratumoral injection of 20 μg of resiquimod in an orthotopic GL261 model in the absence of resection, improved survival with ~30% of mice clearing their tumor. However, these mice were treated much earlier than in the current study, only 5 days after tumor implant compared to our study that treated 10–14 days after tumor implant. Additionally, the edema/trauma created by tumor debulking has been found to affect drug diffusion[45,46]. Therefore it is likely the larger tumor burden, coupled with increased fluid flow induced by surgery, decreased the efficacy of bolus resiquimod in our study.

A similar immunotherapeutic strategy has shown efficacy against other non-intracranial tumors. Park et al.[55] found local resiquimod delivery via hydrogel in orthotopic breast tumors or subcutaneous lung tumors after resection led to improved tumor clearance compared to soluble resiquimod injection. Interestingly, this improved effect was found despite the release of resiquimod from the hydrogel occurring over only 12 h. Upon investigation into the immunological mechanism, Park et al. determined that anti-tumor effect is driven by IFN-I and both innate and adaptive arms of the immune system are required. This is consistent with our finding that Ace-Resi is ineffective in Nu/Nu and Ifnar$^{-/-}$ models. However, it should be noted that hydrogels may have limited application for GBM treatment as there have been reports of adverse mass effects for patients[61-64].

Recently, Turco et al.[65] evaluated a systemic nano formulation of resiquimod against orthotopic GL261 tumors without resection. Utilizing three intravenous administrations of resiquimod nanoparticles (a total dose of 600 μg of resiquimod), led to 43% long-term survivors. It is worth noting that this is comparable to the 80%, 50%, and 60% long-term survivors we achieved with a single administration of 60-, 12-, and 6-fold lower resiquimod dose, respectively, suggesting local administration allows for dose-sparing. This bolsters the strength of our results, confirming that resiquimod is a viable treatment for GBM and warrants further investigation.

Consistent with literature, we found that tumor resection has significant immunostimulatory effects[31,32] in that it activated monocytes, reduced TAM frequency, led to neutrophil infiltration, and temporarily decreased Treg populations in the brain. Resection also led to increased CD8$^+$ T cells trafficking to the cLN and brain. However, many of these effects were transient and all mice treated with resection and Ace-Blank scaffolds succumbed to tumor recurrence. In contrast, resection and Ace-Resi treatment was able to match these effects and continue to build upon them with activated microglia, cDCs, B cells, and NK cells in the brain coupled with a prolonged decrease in Tregs and reduction in T cell exhaustion. Ace-Resi also led to sustained DCs trafficking to the cLN and increased costimulatory expression for

antigen presenting cells in the cLN. Additionally, Ace-Resi treatment resulted in early systemic activation of T cells and increased S1P1 expression for T cells in the bone marrow out to day 7.

The promising results from this study present several opportunities for further exploration and improvement. Encouragingly, mice responded well to this therapy, exhibiting minimal weight loss; however, a comprehensive safety analysis will be essential before translation to a clinical setting. Of note, our finding that resiquimod dose is less important than the sustained local release for antitumor effects, suggests that dose reduction could be achieved for improved safety profile while maintaining therapeutic benefit. One drawback of this study is the absence of human data or patient derived xenograft models which may limit the extent to which findings can be generalized to clinical populations. However, the requirement for an intact immune system to observe Ace-Resi activity necessitates the use of immunocompetent preclinical models. Lastly, in this study we utilized a biodegradable polymer scaffold to achieve continuous local stimulation in mice; however, clinically this could be more simply achieved with a catheter (Ommaya reservoir) placed during surgery. This approach could bypass the lengthy FDA approval process for novel biomaterials and provide the added safety benefit of easily suspending treatment if necessary.

In summary, we formulated TLR7/8 agonist, resiquimod, within a biodegradable nanofibrous Ace-DEX scaffold. We found that increased and sustained local concentration of resiquimod in the brain compared to bolus injection. In two murine models of glioma resection and recurrence, GL261 and CT2A, we found that sustained release of resiquimod was necessary to form an anti-tumor immune response and that surviving mice were protected from subsequent tumor challenge. Additionally, we found Ace-Resi improved survival in a model of breast cancer brain metastasis. We observed that sustained local stimulation of TLR7/8 at the time of tumor resection augments resection-mediated disruption to the immunosuppressive TME and induced systemic T cell trafficking. This allows for the recruitment of inflammatory innate immune cells and freshly primed cytotoxic T cells that can effectively suppress and clear residual tumor while forming a lasting immune memory (Fig. 7E).

Methods
Experimental design

The objective of this controlled laboratory experiment was to determine if sustained local TLR7/8 agonism (achieved by formulating small molecule, resiquimod, within a biodegradable polymer scaffold) applied at the time of GBM tumor resection would improve survival. Pharmacokinetic studies confirmed that Ace-Resi extended the duration of resiquimod exposure in the murine brain relative to bolus injection. Mice bearing two different orthotopic luminescent GBM tumors (GL261-mCh-Luc and CT2A-Luc) were utilized for evaluation, as well as confirmation in the same cell line without reporter protein (CT2A-Par). Treatment was also confirmed in a breast cancer brain metastasis model (EO771). Survival was prospectively selected as the primary endpoint, and for luminescent tumors, serial bioluminescence imaging was used to quantify and monitor local tumor recurrence. Formation of an immune memory response towards the tumor was determined by challenging long-term surviving mice with a new inoculate of tumor cells in the contralateral hemisphere, utilizing naïve mice as a control. Immune cell infiltrates were evaluated by flow cytometry after a second tumor challenge. Tolerability of Ace-Resi treatment was assessed by weight loss. For mechanistic studies, flow cytometry and ELISA were used to assess cell populations and serum cytokines, respectively. Athymic (Nu/Nu) and interferon receptor knockout (Ifnar$^{-/-}$) mouse models were utilized to confirm the mechanism.

Sample sizes were determined based on results from prior experiments to ensure statistical significance could be analyzed. One

control mouse was excluded as it died unrelated to tumor burden, and three mice were euthanized as a result of surgical complications. Mice were randomly assigned to treatment groups on the day of surgery. When possible, monitoring mice for survival was done in a blinded manner. Mice were evaluated regularly and euthanized if they reached humane endpoints.

Cell culture

GL261 cells were engineered to express mCherry-firefly luciferase (mCh-Luc) using previously developed lentiviral vectors to allow for fluorescent and bioluminescent imaging as in our previous study (GL261-mCh-Luc)[66]. Cells were infected for 24 hours and purified by puromycin (Corning, Cat # MT61385RA) selection. Murine glioma cell line CT2A expressing firefly luciferase (CT2A-Luc) was purchased from Millipore Sigma (Cat # SC195). The parental CT2A cell line (CT2A-Par) was a gift from Professor Thomas Seyfried. EO771 cell line (Cat # CRL-3461) was purchased from ATCC. Cells were cultured in high-glucose Dulbecco's Modified Eagle Medium (DMEM, Corning, Cat # 10-013-CV) supplemented with 1% penicillin/streptomycin (Gibco, Cat # 15140122) and 10% fetal bovine serum (FBS, Corning, Cat # 35-015-CV).

Mice

All animal protocols were approved by the University of North Carolina at Chapel Hill Institutional Animal Care and Use Committee (IACUC), and care of mice was in accordance with the standards set forth by the National Institutes of Health Guide for the Care and Use of Laboratory Animals, and the American Veterinary Medical Association. Experimental and control animals were co-housed in a specific pathogen-free/SPF animal facility with 12 hour light/dark cycle 70 °F temperature and 50% humidity. Female C57BL/6 mice age 7–10 weeks from Charles River (stock # 027) were utilized for GL261 models, and Jackson Labs (stock # 00064) for CT2A and EO771 models. Female Nu/Nu (Nu-$Foxn1^{nu}$) mice age 7–10 weeks were obtained from the UNC Lineberger Comprehensive Cancer Center Preclinical Research Unit; this strain is commercially available from Charles River (stock # 088). Male and female $Ifnar1^{-/-}$ mice on a C57BL/6 background age 7–10 weeks were bred in Professor Helen Lazear's lab and generously provided as a kind gift; this strain is commercially available from Jackson Labs (stock # 032045-JAX). Tumor volumes were not directly measured, as tumors were intracranial. Mice were evaluated regularly and euthanized by carbon dioxide asphyxiation and cervical dislocation if they reached humane endpoints as defined by a loss of 20% body weight, signs of distress (facial grimace, hunch), or neurologic symptoms (gait abnormality, head tilt).

Scaffold fabrication

To generate the hydrophobic biopolymer Ace-DEX, dextran (450-650 kDa, Sigma, Cat # 31392) and pyridinium p-toluenesulfonate (1.55% wt/wt, Sigma, Cat # 232238) were dissolved in dimethyl sulfoxide (DMSO, Sigma, Cat # 276855) and reacted with 2-ethoxypropene (20% v/v, Matrix Scientific, Cat # 70378) under anhydrous conditions for 15 minutes. The resulting polymer was precipitated in basic water (400 μL of triethylamine in 1 L of deionized water) and lyophilized. Ace-DEX was dissolved in ethanol (Fisher Cat # 04-355-224) and centrifuged to remove impurities. Then the polymer was re-precipitated in basic water, lyophilized, and stored at -20°C. Cyclic acetal coverage (CAC) was determined to be 31% by nuclear magnetic resonance (NMR, Varian Inova 400)[43].

To formulate resiquimod scaffold, Ace-DEX was dissolved at a concentration of 300 mg/mL in a tri-solvent system consisting of dichloromethane (Fisher, Cat # D37-20), hexafluoro-2-propanol (Sigma, Cat # 105228), and butanol (Sigma, Cat # 360465) at a ratio of 30%, 30%, and 40% v/v respectively. Resiquimod (10% wt/wt, Accel PharmTech, Cat # XP2356) was added to the polymer solution and 1 mL was extruded from a glass syringe with a 21-guage needle at a flow

rate of 1 mL per hour. A voltage bias (± 7 kV direct current) was applied across the needle and a metal collection plate. The resulting scaffold (termed Ace-Resi) was retrieved from the collection plate and stored at -20°C until further use. A scaffold without any resiquimod was fabricated similarly as a control (termed Ace-Blank).

Scaffold characterization

Electrospun scaffolds were evaluated by scanning electron microscopy to elucidate fiber morphology. A small piece of each scaffold was mounted on aluminum stubs using carbon tape, sputter coated with palladium and imaged at 2 kV on a Hitachi S-4700 Cold Cathode Field Emission Scanning Electron Microscope (Hitachi High-Technologies, Krefeld, Germany).

To measure resiquimod loading, scaffold samples were weighed, dissolved in DMSO and the absorbance at 260 nm was compared to a standard curve. Resiquimod encapsulation efficiency was defined as the amount of measured resiquimod divided by the theoretical resiquimod loaded. Resiquimod release and scaffold mass loss were determined by adding pre-weighed scaffold samples to a sink of phosphate buffered saline (PBS, pH 7.4) agitated at 37 °C. At specific time points, scaffold samples were removed, washed with basic water, lyophilized, and re-weighed to determine the total scaffold mass loss. Scaffold mass loss was calculated according to Supp Equation 1. Each scaffold sample was then dissolved in DMSO, and the absorbance at 260 nm was compared against a standard curve to determine the amount of resiquimod retained in each sample. Resiquimod release was calculated according to Supp Equation 2. Ace-Resi and Ace-Blank scaffolds were tested for endotoxin using Pierce Chromogenic Endotoxin Quant Kit (Cat # A39553) according to manufacturer guidelines, and both measured less than 0.1 EU per mg of scaffold.

To assess the pharmacokinetics of resiquimod released from Ace-Resi/fast within the mouse brain compared to bolus soluble injection, experimental groups were applied to a resection cavity created in the right frontal lobe in a non-tumor-bearing C57BL/6 mouse. At 1 hour, 6 hour, 1, 3, and 7 days, mice were euthanized, and the brain and plasma were collected. Any remaining scaffold was removed from the brain. The removed scaffold was lyophilized, dissolved in DMSO, and evaluated by fluorescence (excitation 260 nm, emission 370 nm) against a standard curve to quantify the percentage of resiquimod retained within the remaining scaffold.

Plasma samples and brain tissue were snap frozen. Brain tissue was homogenized in PBS using 1.4 mm porcelain homogenization beads and diluted in PBS for a 4x dilution. Samples were analyzed with LC-MS/MS to measure the concentration of resiquimod. The lower limit of quantification for resiquimod in the brain was 1 ng per gram of tissue and in plasma was 1 ng per mL.

Mouse tumor models

For all surgical procedures, mice were anesthetized by vapor isoflurane. Bupivacaine was utilized for local analgesia, and meloxicam (5 mg/kg) was administered before surgery and once daily for the following 3 days. A model of GBM resection and recurrence was used to evaluate drug-loaded scaffolds similar to those previously described[37]. Complete timelines for all studies are in the main text or supplement (Figs. 2A, 3A, Supplementary Figs. 2A, 3A, 5A, 5D, 15A) and sample sizes for each study are detailed in Supplementary Table 2. Tumor cells were injected (either GL261-mCh-Luc, CT2A-Luc, CT2A-Par, or EO771) at 1×10^5 cells in 2 μL of PBS at a rate of 1 μL per minute into the right frontal lobe of the brain via burr hole approximately 2 mm lateral of bregma and 0.5 mm below the dura. For luminescent tumors, growth was monitored by bioluminescent imaging (Perkin Elmer IVIS Spectrum In Vivo Imaging System) with XenoLight D-luciferin substrate (0.15 mg/kg, Revvity, Cat # 122799). Seven to 14 days after implantation, a cranial window approximately 3 mm in diameter was created around the initial burr hole. Tumors were then

partially resected, treatment was applied to the surgical cavity, and the skin was closed with tissue adhesive (Fisher, Cat # NC0846393). For mice treated with a bolus soluble resiquimod, 100 µg of resiquimod in 5 µL of PBS and DMSO (80%, 20% v/v, respectively) was injected into the exposed brain tissue of the resection cavity. For mice treated with scaffolds, the scaffolds were placed into the resection cavity. The resiquimod dose implanted via Ace-Resi scaffolds was controlled by changing the mass of the scaffold implanted, knowing the empirical drug loading. With a 9.5% w/w loaded scaffold, a 100 µg dose of resiquimod would require 1.05 mg of scaffold, whereas a 10 µg dose of resiquimod would require 0.11 mg of scaffold. Mice were monitored for tumor recurrence and survival. Serial bioluminescent imaging was used to quantify tumor growth.

To assess for a memory immune response in GL261-mCh-Luc and CT2A-Luc studies, long-term survivors were challenged with tumors (2×10^5 GL261-mCh-Luc or CT2A-Luc) in the contralateral hemisphere 9−10 weeks after initial resection and treatment. As a control, naïve mice were also implanted with tumors. Mice were followed for survival, and 6−7 weeks later, survivors were re-challenged again in the contralateral hemisphere. One week after the second challenge, mice were euthanized, and brain lymphocytes were analyzed by flow cytometry. Whole brains were removed and dissociated via homogenization in Hank's buffered salt solution (HBSS). Brain homogenate was resolved with a 70%, 30% percoll gradient, collecting single cells at the interface.

For the CT2A-Par study, survivors were challenged with 2×10^5 CT2A-Par tumors in the contralateral hemisphere 9 weeks after resection and treatment. One week after tumor challenge, mice were euthanized, and brains and spleens were collected. Leukocytes were isolated from the pooled brains, and CD8 + T cells were isolated from the spleen via magnetic bead separation (Miltenyi, Cat # 130-104-075). Additionally, as a control, a healthy naïve mouse was also euthanized, and $CD8^+$ T cells were isolated from the spleen. Effector cells from both groups were expanded through 48 hr culture on CD3 and CD28 antibody-coated plates (0.5 µg per well, 4 hr incubation at 37 °C). For long-term survivors, brain leukocytes (accounting for 5% of the total effector population) and $CD8^+$ T cells isolated from spleen (accounting for 95% of the effector population) were cocultured with CT2A-Par cells at various ratios. For naïve mice, $CD8^+$ T cells from the spleen (accounting for 100% of the effector population) were cocultured with CT2A-Par cells at various ratios. Media was collected at 24 hours from the coculture and evaluated for IFN-γ by ELISA (Biolegend, Cat # 430801).

Evaluation of immunological effects

Mice were implanted with CT2A-Luc tumors in the right frontal lobe as described above. Two weeks later, tumors were resected, and scaffolds were implanted with the following groups: Ace-Blank, Ace-Resi 100 µg. As controls, a subset of mice with and without tumors did not undergo resection, tumor and healthy groups, respectively. At days 1, 3, 7, and 10 following resection, mice were euthanized. Brain, superficial cervical lymph nodes, spleen, bone marrow, and blood were collected for leukocyte analysis. Serum was also collected, and cytokines were measured by ELISA according to manufacturer guidelines: IFN-β (R&D Systems, Cat # DY8234-05), TNF (Biolegend, Cat # 430901), IFN-γ (Biolegend, Cat # 430801).

Superficial cervical lymph nodes (pooled from right and left sides), spleen, and bone marrow (extruded from a single femur) were harvested. Single-cell suspensions were generated by grinding through a 70 µm cell strainer. Red blood cells were lysed from spleen and bone marrow samples with ACK lysis buffer. All cell suspensions were washed with FACs buffer (PBS + 2% FBS), then passed through another 70 µm strainer.

Blood was collected into both K3EDTA-coated (Greiner, Cat # 450475) and serum separator tubes (Greiner, Cat # 450472). Serum was stored at -80 °C for later use. Fifty microliters of blood from K3EDTA tubes was treated with ACK lysis buffer to remove red blood cells. The cell suspension was then washed with FACs buffer.

For S1P1 staining, bone marrow (extruded from a single femur) was harvested into S1P1 buffer (500 mL PBS, 5 mL 10% buffered neutral formalin, 2 mL 0.5 M EDTA, 2.5 g bovine serum albumin) to fix cells immediately. Single-cell suspensions were generated by grinding through a 70-µm cell strainer in S1P1 buffer. Red blood cells were lysed with ACK lysis buffer. Cell suspensions were washed with S1P1 buffer and passed through another 70 µm strainer. Cells were washed twice in FACS buffer, stained for 30 minutes on ice, then washed twice and resuspended in FACS buffer.

Whole brains were removed and dissociated via homogenization in HBSS. Brain homogenate was suspended in 30% Percoll, and the cell pellet was collected. Red blood cells were lysed with ACK lysis buffer. Cell suspensions were washed twice in FACS buffer and passed through a 70 µm strainer.

Following the generation of single-cell suspensions, cells were divided based on downstream application (either surface staining or intracellular cytokine staining (ICCS)). For the identification and exclusion of dead cells in all flow analysis, samples were stained with eBioscience Fixable Viability Dye (Invitrogen, Cat # 65-0866-018) diluted 1:1000 in FACS buffer for 30 minutes on ice, then washed twice with FACS buffer. All samples were acquired using either an Attune NxT flow cytometer (ThermoFisher) or an LSRFortessa flow cytometer (Becton Dickinson). Flow data analysis was performed using FlowJo (Becton Dickinson). All samples were subject to sequential debris, doublet, and dead cell removal prior to analysis. A complete list of antibody clones, fluorochrome conjugates, vendors, and dilutions is included in Supplementary Table 3.

For brain lymphocyte panel, cells were treated with brefeldin A (5 µg/mL, Biolegend, Cat # 420601) and monensin (2 µM, Biolegend, Cat # 420701) with and without phorbol 12-myristate 13-acetate (50 ng/mL, Sigma, Cat # P8139) and ionomycin (500 ng/mL, Sigma, Cat # I0634) for 4 hours at 37 °C.

For systemic lymphocyte and systemic counts panels (involving only surface stains), cells were washed twice in FACS buffer, then stained for 30 minutes on ice in FACS buffer, resuspended in 1% formaldehyde in PBS for 30 minutes on ice, then washed twice and resuspended in FACS buffer. All other panels employed ICCS, where cells were then fixed and permeabilized for 30 minutes on ice using the eBioscience Foxp3 / Transcription Factor Staining Buffer Set (Thermo Fisher, Cat # 00-5523-00), washed twice with permeabilization buffer, then stained with a mixture of fluorochrome-conjugated antibodies diluted in permeabilization buffer for 30 minutes at room temperature, washed twice with permeabilization buffer and resuspended in FACS buffer. Gating strategies for flow panels are in Supplementary Figs. 16–20.

FlowSOM UMAP analysis

Following the gating strategy in Supplementary Fig. 21, the flow cytometry data from the brain for the leukocyte panel were down-sampled on a CD45+ gate to ensure each animal was represented equally. Files were concatenated to generate UMAP figures clustered by FlowSOM defined via a heatmap in Supplementary Fig. 21.

Statistical analysis

In all figures, data are presented as mean ± standard deviation unless otherwise stated. Each data point represents measurements taken from distinct biological samples. Statistical analysis was performed using GraphPad Prism (La Jolla, CA). Mouse survival curves were evaluated by log-rank (Mantel-Cox) test. Statistical significance for flow cytometry data was determined by two-tailed unpaired t-test or one-way ANOVA, with multiple comparisons using Tukey's post hoc test.

Reporting summary

Further information on research design is available in the Nature Portfolio Reporting Summary linked to this article.

Data availability

All data are included in the Supplementary Information or available from the authors, as are unique reagents used in this Article. The raw numbers for charts and graphs are available in the Source Data file whenever possible. Source data are provided with this paper.

References

1. Adamson, C. et al. Glioblastoma multiforme: a review of where we have been and where we are going. *Expert Opin. Investig. Drugs* **18**, 1061–1083 (2009).
2. Erpolat, O. P. et al. Outcome of newly diagnosed glioblastoma patients treated by radiotherapy plus concomitant and adjuvant temozolomide: a long-term analysis. *Tumori* **95**, 191–197 (2009).
3. Stupp, R. et al. Effects of radiotherapy with concomitant and adjuvant temozolomide versus radiotherapy alone on survival in glioblastoma in a randomised phase III study: 5 year analysis of the EORTC-NCIC trial. *Lancet Oncol.* **10**, 459–466 (2009).
4. Bastiancich, C., Malfanti, A., Préat, V. & Rahman, R. Rationally designed drug delivery systems for the local treatment of resected glioblastoma. *Adv. Drug Deliv. Rev.* **177**, 113951 (2021).
5. Wang, P. P., Frazier, J. & Brem, H. Local drug delivery to the brain. *Adv. Drug Deliv. Rev.* **54**, 987–1013 (2002).
6. Woodring, R. N., Gurysh, E. G., Bachelder, E. M. & Ainslie, K. M. Drug delivery systems for localized cancer combination therapy. *ACS Appl. Bio Mater.* **6**, 934–950 (2023).
7. Fleming, A. B. & Saltzman, W. M. Pharmacokinetics of the carmustine implant. *Clin. Pharmacokinet.* **41**, 403–419 (2002).
8. Iuchi, T. et al. Long-term effectiveness of Gliadel implant for malignant glioma and prognostic factors for survival: 3 year results of a postmarketing surveillance in Japan. *Neurooncol. Adv.* **4**, vdab189 (2022).
9. Bregy, A. et al. The role of Gliadel wafers in the treatment of high-grade gliomas. *Expert Rev. Anticancer Ther.* **13**, 1453–1461 (2013).
10. McGranahan, T., Therkelsen, K. E., Ahmad, S. & Nagpal, S. Current state of immunotherapy for treatment of glioblastoma. *Curr. Treat. Options Oncol.* **20**, 24 (2019).
11. Reardon, D. A. et al. Effect of nivolumab vs bevacizumab in patients with recurrent glioblastoma: the checkmate 143 phase 3 randomized clinical trial. *JAMA Oncol.* **6**, 1003–1010 (2020).
12. Markert, J. M. et al. A phase 1 trial of oncolytic HSV-1, G207, given in combination with radiation for recurrent GBM demonstrates safety and radiographic responses. *Mol. Ther.* **22**, 1048–1055 (2014).
13. Bogdahn, U. et al. Targeted therapy for high-grade glioma with the TGF-β2 inhibitor trabedersen: results of a randomized and controlled phase IIb study. *Neuro Oncol.* **13**, 132–142 (2010).
14. Brandes, A. A. et al. A phase II randomized study of galunisertib monotherapy or galunisertib plus lomustine compared with lomustine monotherapy in patients with recurrent glioblastoma. *Neuro-Oncol.* **18**, 1146–1156 (2016).
15. Butowski, N. et al. Orally administered colony stimulating factor 1 receptor inhibitor PLX3397 in recurrent glioblastoma: an ivy foundation early phase clinical trials consortium phase II study. *Neuro-Oncol.* **18**, 557–564 (2015).
16. Butowski, N. et al. A phase II clinical trial of poly-ICLC with radiation for adult patients with newly diagnosed supratentorial glioblastoma: a North American Brain Tumor Consortium (NABTC01-05). *J. Neuro Oncol.* **91**, 175 (2008).
17. Woroniecka, K. et al. T-cell exhaustion signatures vary with tumor type and are severe in glioblastoma. *Clin. Cancer Res.* **24**, 4175–4186 (2018).
18. Sampson, J. H., Gunn, M. D., Fecci, P. E. & Ashley, D. M. Brain immunology and immunotherapy in brain tumours. *Nat. Rev. Cancer* **20**, 12–25 (2020).
19. Chongsathidkiet, P. et al. Sequestration of T cells in bone marrow in the setting of glioblastoma and other intracranial tumors. *Nat. Med* **24**, 1459–1468 (2018).
20. Thorsson, V. et al. The immune landscape of cancer. *Immunity* **48**, 812–830.e814 (2018).
21. Patel, A. P. et al. Single-cell RNA-seq highlights intratumoral heterogeneity in primary glioblastoma. *Science* **344**, 1396–1401 (2014).
22. O'Rourke, D. M. et al. A single dose of peripherally infused EGFRvIII-directed CAR T cells mediates antigen loss and induces adaptive resistance in patients with recurrent glioblastoma. *Sci. Transl. Med.* **9**, eaaa0984 (2017).
23. Brown, C. E. et al. Regression of glioblastoma after chimeric antigen receptor T-cell therapy. *N. Engl. J. Med.* **375**, 2561–2569 (2016).
24. Hussain, S. F. et al. The role of human glioma-infiltrating microglia/macrophages in mediating antitumor immune responses. *Neuro Oncol.* **8**, 261–279 (2006).
25. Parney, I. F., Waldron, J. S. & Parsa, A. T. Flow cytometry and in vitro analysis of human glioma–associated macrophages. *J. Neurosurg.* **110**, 572–82 (2009).
26. Rolfo, C., Giovannetti, E., Martinez, P., McCue, S. & Naing, A. Applications and clinical trial landscape using Toll-like receptor agonists to reduce the toll of cancer. *npj Precis. Oncol.* **7**, 26 (2023).
27. Abarca-Merlin, D., Maldonado-Bernal, C. & Alvarez-Arellano, L. Toll-like receptors as therapeutic targets in central nervous system tumors. *BioMed. Res. Int.* **2019**, 5286358 (2019).
28. Grauer, O. M. et al. TLR ligands in the local treatment of established intracerebral murine gliomas. *J. Immunol.* **181**, 6720–6729 (2008).
29. Kudo, Y. et al. Suppressed immune microenvironment and repertoire in brain metastases from patients with resected non-small-cell lung cancer. *Ann. Oncol.* **30**, 1521–1530 (2019).
30. Tang, F., Tie, Y., Tu, C. & Wei, X. Surgical trauma-induced immunosuppression in cancer: recent advances and the potential therapies. *Clin. Transl. Med.* **10**, 199–223 (2020).
31. Choi, S. H. et al. Tumor resection recruits effector T cells and boosts therapeutic efficacy of encapsulated stem cells expressing IFNβ in glioblastomas. *Clin. Cancer Res.* **23**, 7047–7058 (2017).
32. Khalsa, J. K. et al. Immune phenotyping of diverse syngeneic murine brain tumors identifies immunologically distinct types. *Nat. Commun.* **11**, 3912 (2020).
33. Bakos, O., Lawson, C., Rouleau, S. & Tai, L.-H. Combining surgery and immunotherapy: turning an immunosuppressive effect into a therapeutic opportunity. *J. Immunother. Cancer* **6**, 86 (2018).
34. Cloughesy, T. F. et al. Neoadjuvant anti-PD-1 immunotherapy promotes a survival benefit with intratumoral and systemic immune responses in recurrent glioblastoma. *Nat. Med.* **25**, 477–486 (2019).
35. Marabelle, A., Kohrt, H., Caux, C. & Levy, R. Intratumoral immunization: a new paradigm for cancer therapy. *Clin. Cancer Res.* **20**, 1747–1756 (2014).
36. Borteh, H. M. et al. Electrospun acetalated dextran scaffolds for temporal release of therapeutics. *Langmuir* **29**, 7957–7965 (2013).
37. Graham-Gurysh, E. et al. Sustained delivery of doxorubicin via acetalated dextran scaffold prevents glioblastoma recurrence after surgical resection. *Mol. Pharm.* **15**, 1309–1318 (2018).
38. Graham-Gurysh, E. G. et al. Tumor responsive and tunable polymeric platform for optimized delivery of paclitaxel to treat glioblastoma. *Acs Appl Mater. Inter* https://doi.org/10.1021/acsami.0c04102 (2020).
39. Graham-Gurysh, E. G. et al. Synergistic drug combinations for a precision medicine approach to interstitial glioblastoma therapy. *J. Control Release* **323**, 282–292 (2020).
40. Junkins, R. D. et al. A robust microparticle platform for a STING-targeted adjuvant that enhances both humoral and cellular

immunity during vaccination. *J. Controlled Release. Off. J. Controlled Release. Soc.* **270**, 1–13 (2018).

41. Kanthamneni, N. et al. Enhanced stability of horseradish peroxidase encapsulated in acetalated dextran microparticles stored outside cold chain conditions. *Int. J. Pharm.* **431**, 101–110 (2012).

42. Bachelder, E. M., Beaudette, T. T., Broaders, K. E., Dashe, J. & Fréchet, J. M. J. Acetal-derivatized dextran: an acid-responsive biodegradable material for therapeutic applications. *J. Am. Chem. Soc.* **130**, 10494–10495 (2008).

43. Kauffman, K. J. et al. Synthesis and characterization of acetalated dextran polymer and microparticles with ethanol as a degradation product. *ACS Appl. Mater. Interfaces* **4**, 4149–4155 (2012).

44. Broaders, K. E., Cohen, J. A., Beaudette, T. T., Bachelder, E. M. & Frechet, J. M. Acetalated dextran is a chemically and biologically tunable material for particulate immunotherapy. *Proc. Natl. Acad. Sci. USA* **106**, 5497–5502 (2009).

45. Arifin, D. Y., Lee, K. Y., Wang, C. H. & Smith, K. A. Role of convective flow in carmustine delivery to a brain tumor. *Pharm. Res.* **26**, 2289–2302 (2009).

46. Tan, W. H. K., Lee, T. & Wang, C.-H. Simulation of intratumoral release of etanidazole: effects of the size of surgical opening. *J. Pharm. Sci. Us* **92**, 773–789 (2003).

47. Van Gassen, S. et al. FlowSOM: Using self-organizing maps for visualization and interpretation of cytometry data. *Cytom. A* **87**, 636–645 (2015).

48. Deng, Y. et al. Microglia and macrophage metabolism: a regulator of cerebral gliomas. *Cell Biosci.* **14**, 49 (2024).

49. Ohue, Y. & Nishikawa, H. Regulatory T (Treg) cells in cancer: can treg cells be a new therapeutic target?. *Cancer Sci.* **110**, 2080–2089 (2019).

50. van der Leun, A. M., Thommen, D. S. & Schumacher, T. N. CD8(+) T cell states in human cancer: insights from single-cell analysis. *Nat. Rev. Cancer* **20**, 218–232 (2020).

51. Cibrián, D. & Sánchez-Madrid, F. CD69: from activation marker to metabolic gatekeeper. *Eur. J. Immunol.* **47**, 946–953 (2017).

52. Kamphuis, E., Junt, T., Waibler, Z., Forster, R. & Kalinke, U. Type I interferons directly regulate lymphocyte recirculation and cause transient blood lymphopenia. *Blood* **108**, 3253–3261 (2006).

53. Stathopoulos, A. et al. Development of immune memory to glial brain tumors after tumor regression induced by immunotherapeutic toll-like receptor 7/8 activation. *Oncoimmunology* **1**, 298–305 (2012).

54. Bhagchandani, S., Johnson, J. A. & Irvine, D. J. Evolution of toll-like receptor 7/8 agonist therapeutics and their delivery approaches: from antiviral formulations to vaccine adjuvants. *Adv. Drug Deliv. Rev.* **175**, 113803 (2021).

55. Park, C. G. et al. Extended release of perioperative immunotherapy prevents tumor recurrence and eliminates metastases. *Sci. Transl. Med.* **10**, eaar1916 (2018).

56. Lu, R. et al. Formulation and preclinical evaluation of a toll-like receptor 7/8 agonist as an anti-tumoral immunomodulator. *J. Control Release* **306**, 165–176 (2019).

57. Zhang, H. et al. Development of thermosensitive resiquimod-loaded liposomes for enhanced cancer immunotherapy. *J. Control Release* **330**, 1080–1094 (2021).

58. Pockros, P. J. et al. Oral resiquimod in chronic HCV infection: safety and efficacy in 2 placebo-controlled, double-blind phase IIa studies. *J. Hepatol.* **47**, 174–182 (2007).

59. Daniels, G. A. et al. Phase I open-label, dose-escalation study of ANA773 tosylate, an oral prodrug of a toll-like receptor-7 agonist, in patients with advanced solid tumors. *J. Clin. Oncol.* **29**, 2524–2524 (2011).

60. Zahr, N. M., Zhao, Q., Goodcase, R. & Pfefferbaum, A. Systemic administration of the TLR7/8 agonist resiquimod (R848) to mice is associated with transient, in vivo-detectable brain swelling. *Biology* **11**, 274 (2022).

61. Gong, Y. et al. Role of mass effect and trehalose on early erythrolysis after experimental intracerebral hemorrhage. *J. Neurochem.* **160**, 88–99 (2022).

62. Gong, Y. et al. Establishment of an experimental intracerebral haemorrhage model for mass effect research using a thermosensitive hydrogel. *Sci. Rep.* **9**, 13838 (2019).

63. Blackburn, S. L. & Smyth, M. D. Hydrogel-induced cervicomedullary compression after posterior fossa decompression for chiari malformation: case report. *J. Neurosurg. Pediatrics PED* **106**, 302–304 (2007).

64. Raymond, J. et al. Hydrogel versus bare platinum coils in patients with large or recurrent aneurysms prone to recurrence after endovascular treatment: a randomized controlled trial. *Am. J. Neuroradiol.* **38**, 432–441 (2017).

65. Turco, V. et al. T cell-independent eradication of experimental glioma by intravenous TLR7/8-agonist-loaded nanoparticles. *Nat. Commun.* **14**, 771 (2023).

66. Okolie, O. et al. Reactive astrocytes potentiate tumor aggressiveness in a murine glioma resection and recurrence model. *Neuro Oncol.* **18**, 1622–1633 (2016).

Acknowledgements

Author contributions

E.G.G., S.R.S., E.M.B., P.E.F., and K.M.A. designed the experiments. E.S.P. synthesized and characterized the polymer and scaffolds. K.A.H. and W.C.Z. performed pharmacokinetic analysis. E.G.G., R.N.W., and K.M.M. performed animal studies. E.G.G., R.N.W., E.S.P., S.E.M., N.R.L., G.S., L.A.H., A.T.H., A.M.L., G.L.W., and C.T.M. assisted in tissue harvesting and organ processing. S.R.S., C.J.G., N.R.L., and S.E.M. acquired and analyzed flow cytometry data. E.G.G., S.R.S., R.N.W., N.R.L., and S.E.M. made figures. K.M.A., E.M.B., W.C.Z., S.D.H., P.E.F. supervised experiments. E.G.G. and S.R.S. wrote the manuscript with input from all coauthors.

Competing interests

The authors declare no competing interests.

Additional information

Supplementary information The online version contains supplementary material available at https://doi.org/10.1038/s41467-025-63692-9.

Correspondence and requests for materials should be addressed to Kristy M. Ainslie.

Peer review information *Nature Communications* thanks Michael Breckwoldt and the other, anonymous, reviewer(s) for their contribution to the peer review of this work. A peer review file is available.

Reprints and permissions information is available at http://www.nature.com/reprints

Publisher's note Springer Nature remains neutral with regard to jurisdictional claims in published maps and institutional affiliations.

[1]Division of Pharmacoengineering and Molecular Pharmaceutics, Eshelman School of Pharmacy, University of North Carolina at Chapel Hill, Chapel Hill, NC, USA. [2]Joint Department of Biomedical Engineering, University of North Carolina at Chapel Hill and North Carolina State University, Chapel Hill, NC, USA. [3]Department of Microbiology and Immunology, UNC School of Medicine, University of North Carolina at Chapel Hill, Chapel Hill, NC, USA. [4]Division of Pharmacotherapy and Experimental Therapeutics, Eshelman School of Pharmacy, University of North Carolina at Chapel Hill, Chapel Hill, NC, USA. [5]Lineberger Comprehensive Cancer Center, University of North Carolina at Chapel Hill, Chapel Hill, NC, USA. [6]Preston Robert Tisch Brain Tumor Center, Duke University Medical Center, Durham, NC, USA. [7]Department of Neurosurgery, Duke University Medical Center, Durham, NC, USA. [8]Department of Pathology, Duke University Medical Center, Durham, NC, USA. ✉e-mail: ainsliek@email.unc.edu